

The Properties of Fossil Groups of Galaxies

Paul Eigenthaler* and Werner W. Zeilinger

Institut für Astronomie, Universität Wien, Türkenschanzstraße 17, A-1180 Wien, Austria

The dates of receipt and acceptance should be inserted later

Key words galaxies: dwarf – galaxies: elliptical and lenticular, cD – galaxies: evolution – galaxies: interactions

Numerical simulations as well as optical and X-ray observations over the last few years have shown that poor groups of galaxies can evolve to what is called a fossil group. Dynamical friction as the driving process leads to the coalescence of individual galaxies in ordinary poor groups leaving behind nothing more than a central, massive elliptical galaxy supposed to contain the merger history of the whole group. Due to merging timescales for less-massive galaxies and gas cooling timescales of the X-ray intragroup medium exceeding a Hubble time, a surrounding faint-galaxy population having survived this galactic cannibalism as well as an extended X-ray halo similar to that found in ordinary groups, is expected. Recent studies suggest that fossil groups are very abundant and could be the progenitors of brightest cluster galaxies (BCGs) in the centers of rich galaxy clusters. However, only a few objects are known to the literature. This article aims to summarize the results of observational fossil group research over the last few years and presents ongoing work by the authors. Complementary to previous research, the SDSS and RASS surveys have been cross-correlated to identify new fossil structures yielding 34 newly detected fossil group candidates. Observations with ISIS at the 4.2m William Herschel Telescope on La Palma have been carried out to study the stellar populations of the central ellipticals of 6 fossil groups. In addition multi-object spectroscopy with VLTs VIMOS has been performed to study the shape of the OLF of one fossil system.

© WILEY-VCH Verlag GmbH & Co. KGaA, Weinheim

1 Introduction

Redshift surveys have shown that galaxies in the nearby universe are not randomly distributed in space but rather found in aggregates, so called galaxy groups (Geller & Huchra 1983, Tully 1987). Basically galaxy groups can be divided into three major classes that differ mainly in their optical and physical characteristics: poor groups, compact groups, and fossil groups.

Poor or loose groups with a space density of $\sim 10^{-5} \text{ Mpc}^{-3}$ (Nolthenius & White, 1987) resemble simple multiplets of galaxies, represent the most common class and are simply referred to as galaxy groups. They are comprised of approximately 50 members, including numerous dwarf galaxies and take up typical diameters of $\sim 1.5 \text{ Mpc}$. Compact groups with a space density of $\sim 1-2 \times 10^{-6} \text{ Mpc}^{-3}$ (Hickson 1982) are less abundant and typically made up of only 4 to 5 bright galaxies strongly interacting with each other due to their mutual gravitational attraction causing tidal forces to form tails around closely interacting members. Since today, about 1000 compact groups have been classified (Hickson 1997). Fossil groups are characterised through a dominating central bright elliptical galaxy comparable to cD galaxies in clusters surrounded by a diffuse and extended X-ray halo together with a significant fainter galaxy population. Recent studies have estimated space densities of fossil systems in the local universe to be $\sim 1-4 \times 10^{-6} \text{ Mpc}^{-3}$, comparable to HCGs. Besides the fact that the vast majority of galaxies in the universe appear to be located

in groups, these systems play also a key role in our understanding of galaxy evolution. Since the masses of groups are comparatively small ($\sim 10^{13} \text{ M}_{\odot}$) with respect to the richer clusters ($\sim 10^{14} \text{ M}_{\odot}$), the virial theorem implies lower values for the group velocity dispersions favoring galaxy interactions leading to the coalescence of individual galaxies, galaxy merging.

Numerical simulations have shown that this cannibalism can proceed as long as a single, massive elliptical galaxy remains as final product of multiple merging events (Barnes 1989) on a timescale of a few gigayears. The physical origin behind the merging of galaxies is explained by dynamical friction of the group member galaxies with the group dark-matter halo and acts not for all types of galaxies similarly effective. According to the description of dynamical friction by Chandrasekhar (1943), the friction force is strongly mass dependent leading to longer merging timescales (see Binney & Tremaine p.429) for less massive galaxies which therefore should have survived this galactic cannibalism up to now. Moreover, the hot X-ray gas, as found in $\sim 50\%$ of all known galaxy groups (not correlated with individual group members but rather diffusely distributed following the global gravitational group potential (Mulchaey 2000)) is also expected to be observed in this state of hierarchical galaxy evolution since gas temperatures and electron densities of a typical intragroup medium with $T \sim 10^7 \text{ K}$ and $n_e \sim 10^{-3} \text{ cm}^{-3}$ suggest gas cooling timescales $\tau_{\text{cool}} \propto n_e^{-1} T_g^{1/2}$ exceeding the age of the universe. Thus, one claims that *fossil groups* represented by a central bright, massive elliptical galaxy surrounded by a diffuse and ex-

* e-mail: eigenthaler@astro.univie.ac.at

tended X-ray halo and a fainter galaxy population are the remnants of what was initially a poor group of galaxies that has been transformed to this old, *fossil* stage of galaxy evolution in low density environments with compact groups acting as likely way station in this evolution. If this scenario is correct then the relative space densities of these three different types of systems give information on their transformation rates. Moreover, Jones et al. (2003) assume that fossil systems constitute of probably 8-20% of all systems with comparable X-ray luminosity ($\geq 10^{42}$ ergs s^{-1}), thus acting also very likely as the site of formation of brightest cluster galaxies (BCGs) before the infall into clusters. Similar optical luminosities of the central ellipticals in fossil groups compared to that of BCGs support this idea. Therefore fossils play a crucial role in our understanding of galaxy evolution in low-density environments and the physical connection between groups and clusters respectively.

The definition of a fossil system as proposed by Jones et al. (2003) was the first real attempt to attribute exact observational characteristics to this class. According to their influential paper a fossil system is a spatially extended X-ray source with an X-ray luminosity from diffuse, hot gas of $L_{X,bol} \geq 10^{42} h_{50}^{-2}$ ergs s^{-1} . The optical counterpart is a bound system of galaxies with $\Delta m_{1,2} \geq 2.0$ mag, where $\Delta m_{1,2}$ is the absolute total magnitude difference in the Johnson R band between the two brightest galaxies in the system within half the projected virial radius. No upper limit is given for the X-ray luminosity or temperature. The ideas behind this classification scheme are simple. The lower limit in X-ray luminosity excludes normal bright elliptical galaxies exhibiting a hot coronal gas component. The magnitude gap of $\Delta m_{1,2} \geq 2.0$ mag for the two brightest galaxies of the group ensures that one single elliptical galaxy dominates the system. Studies of luminosity functions of galaxy groups have shown that this threshold acts as a good criterion to distinguish between poor groups and fossil aggregates since observations have shown that such a high magnitude gap is extremely unlikely to occur in ordinary groups or clusters (Beers et al. 1995).

The first fossil group identified, RX J1340.6+4018, was published in Nature (Ponman et al. 1994). Since then, few other objects have been assigned to this class resulting in a catalogue of 15 fossil systems summarized by Mendes de Oliveira et al. (2006).

However, not all listed objects represent what is typically referred to as fossil group since more massive systems with velocity dispersions in the range of 600 km s^{-1} , thus more appropriate to galaxy clusters, are also present (Cypriano et al. 2006, Mendes de Oliveira et al. 2006). More recently, Santos et al. (2007) have cross-correlated optical and X-ray data from the Sloan Digital Sky Survey (SDSS) (Adelman-McCarthy et al. 2008) and the ROSAT All Sky Survey (RASS) (Voges et al. 1999) respectively to identify new fossil group candidates. Their findings comprise a list of 34 candidates, ranging up to $z = 0.489$. The majority of all known 49 systems ($\sim 86\%$) resides in the northern cele-

Table 1 Fossil galaxy groups as summarized by Mendes de Oliveira et al. (2006). RX denotations refer to ROSAT X-ray sources.

Name	α_{2000}	δ_{2000}	z	$L_{X,bol}^a$
NGC 1132	02 52 51.8	-01 16 29	0.023	1.9
RX J0454.8-1806	04 54 52.2	-18 06 56	0.031	1.9
ESO 306- G 017	05 40 06.7	-40 50 11	0.036	129
RX J1119.7+2126	11 19 43.7	+21 26 50	0.061	1.7
RX J1159.8+5531	11 59 51.4	+55 32 01	0.081	22
CL 1205+44	12 05 53.7	+44 29 46	0.59	180
RX J1256.0+2556	12 56 03.4	+25 56 48	0.232	61.
RX J1331.5+1108	13 31 30.2	+11 08 04	0.081	5.9
RX J1340.6+4018	13 40 33.4	+40 17 48	0.171	25
RX J1416.4+2315	14 16 26.9	+23 15 32	0.137	220.
RX J1552.2+2013	15 52 12.5	+20 13 32	0.136	63
NGC 6034	16 03 32.1	+17 11 55	0.034	0.75
NGC 6482	17 51 48.8	+23 04 19	0.013	2.17
RX J2114.3-6800	21 14 20.4	-68 00 56	0.130	20
RX J2247.4+0337	22 47 29.1	+03 37 13	0.199	41

^a bolometric X-ray luminosity taken in $10^{42} h_{50}^{-2}$ ergs s^{-1}

tial hemisphere whereas only 7 objects ($\sim 14\%$) have been identified in the southern one. The nearest fossil group was identified with the elliptical NGC 6482 at a redshift of $z = 0.013$ (Khosroshahi et al. 2004) while the most distant fossil aggregate was found at $z = 0.59$ combining HST, Chandra and XMM-Newton data (Ulmer et al. 2005, see Fig. 1).

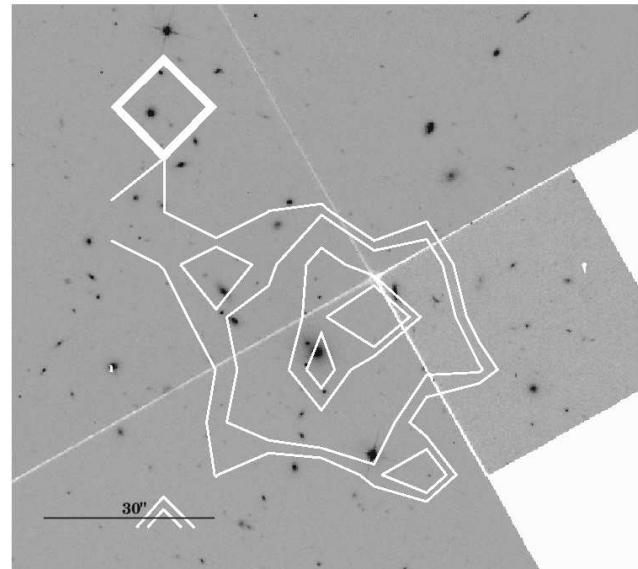


Fig. 1 F702W *HST* image of CL1205+44, the most distant fossil group known. Chandra contours in the range 0.5-8keV indicate the diffuse and extended X-ray gas component. North is up, east is to the left. Taken from Ulmer et al. (2005).

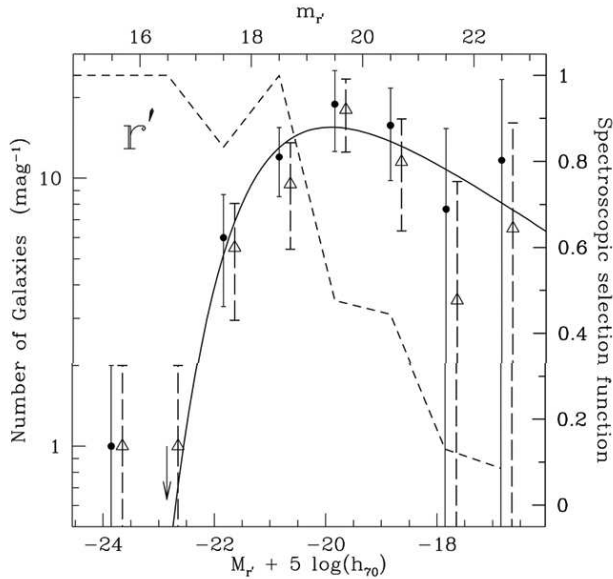


Fig. 2 Luminosity function of the fossil cluster RX J1552.2+2013 in the SDSS r' band. Solid circles show the completeness-corrected number of spectroscopically confirmed members while triangles show photometrically determined members estimated through number counts and statistical background subtraction. The dotted line represents a selection function of the spectroscopic sample while the continuous line shows the best Schechter fit to the spectroscopic sample excluding the brightest galaxy. A clear dip in the LF can be found around $M_{r'} = -18$. Taken from Mendes de Oliveira et al. (2006).

2 The properties of fossil groups

Since the catalogue of known fossil aggregates is only made up of a few objects, an analysis of the optical or X-ray properties of fossil groups has only been carried out for a few systems leaving the formation process of this special class of objects still unclear. This section highlights some of the results that have been obtained over the last few years.

2.1 The luminosity function of fossil galaxy groups

The optical luminosity function (OLF) of fossil groups exhibits a lack of bright galaxies (by definition since fossil systems are characterised as low-density environments with no bright galaxies besides the central elliptical). Thus, the bright end of the OLF of these systems is unusual compared to what is normally observed in poor groups, with too few L^* galaxies present. Few effort has been made so far to study the shape of the OLF at fainter magnitudes. Existing studies focusing on the fainter part of the OLF of fossil galaxy groups have only investigated three fossil systems. Surprisingly, all these aggregates are rather classified as fossil clusters than groups due to their relatively large velocity dispersions (623 km s^{-1} , 584 km s^{-1} , and

565 km s^{-1}) (Cypriano et al. 2006, Mendes de Oliveira et al. 2006, Mendes de Oliveira et al. 2009). Interestingly, besides the expected magnitude gap around L^* galaxies, a dip in the OLF of RX J1552.2+2013 at the transition to dwarf galaxies at $M_{r'} = -18$ has been found (see Fig. 2). Such dips in the OLFs have been observed in several systems, mostly dense, dynamically well-evolved aggregates such as X-ray emitting cD clusters (Valotto et al. 2004) or compact groups of galaxies (Hunsberger et al. 1996), suggesting that there may be more than one mechanism driving the depletion of galaxies in these different environments. Assuming the merger scenario hypothesis from hierarchical galaxy evolution models, the lack of L^* galaxies is explained by dynamical friction, resulting in a deceleration of the orbital velocity of a galaxy which loses its kinetic energy to the surrounding dark matter particles, and subsequent merging. The same physical processes cannot be efficient enough to reproduce the comparatively small number of low-mass galaxies around $M_R = -18$. One explanation for these missing galaxies could be a succession of tidal encounters (Gnedin 2003). If this scenario is correct, one would not expect such a dip in the luminosity functions for less rich galaxy aggregates than the observed fossil cluster, since the galaxy density and thus the tidal stripping efficiency is much lower in these systems. However, RX J1416.4+2315 and RXJ1340.6+4018 do not show any evidence of a dip in the OLF around $M_R = -18$, suggesting that the scenario of fossil group formation is far more complicated than expected. More studies focusing on multi-object spectroscopy of the faint-galaxy population in fossil groups or fossil systems in general is therefore needed.

2.2 Masses and mass-to-light ratios of fossil groups

The symmetric and regular X-ray emission together with the lack of L^* galaxies and the large early-type fraction observed in fossil groups suggest that these systems are old, evolved systems. Thus, from a dynamical point of view, fossil groups should present relaxed, virialized galaxy aggregates. The dynamical properties of the faint-galaxy population of fossil systems studied so far show that the radial velocity distributions exhibit far too high velocity dispersions to be considered as remnants of what was initially a poor group of galaxies and are fairly well fit by a gaussian velocity distribution, indicating relaxed systems. It is feasible to estimate the masses of fossil groups from the gas density and temperature profiles of the extended X-ray gas component assuming the gas distribution to be spherically symmetric and in hydrostatic equilibrium. Then the total gravitational mass is given by

$$M_{\text{grav}}(< r) = -\frac{kT(r)r}{G\mu m_p} \left[\frac{d \ln \rho(r)}{d \ln r} + \frac{d \ln T(r)}{d \ln r} \right] \quad (1)$$

where μ is the mean molecular weight and m_p the proton mass. X-ray studies confirm the high masses derived from the dynamical state of these systems, showing that the intragroup medium of a number of fossil groups is similar to

those of galaxy clusters with temperatures exceeding even 4 keV for some aggregates. These results are inconsistent with the idea that fossil groups are the remains of galactic cannibalism in ordinary groups. Complementary, Yoshioka et al. (2004) has shown that the M/L ratios of four fossil groups reach up to $M/L_B = 1100 M_\odot/L_\odot$ being at least one order of magnitude higher than the typical M/L ratios for groups and clusters of comparable mass supporting the idea that it is unlikely that these systems are the remnants of regular groups and clusters. Other recent studies derive much lower values of M/L, however (e.g. Sun et al. 2004), showing that a general formation scenario for fossil systems is far from understood and further observations in both optical and X-rays are needed to get reliable mass estimates for a higher number of fossil aggregates and to see if all fossil structures resemble cluster-like systems rather than groups.

2.3 Surface brightness profiles of the central ellipticals

The shape of the surface brightness profiles of ellipticals are known to depend on the formation histories of these systems and can thus act as indicators for different imaginable evolution tracks. More precisely, dissipationless merger simulations from Naab & Burkert (2003) have shown that unequal-mass mergers lead to fast rotating, discy ellipticals, while equal mass mergers produce slowly rotating, pressure supported systems. Major mergers between bulge dominated systems result in boxy ellipticals, independent of the mass ratio while merger remnants that subsequently accrete gas are always discy. More recently, it has been shown that the mergers of spiral galaxies alone cannot reproduce the kinematic and photometric properties of very massive ellipticals (Naab, Khochfar & Burkert 2006) nor can they reproduce the observed correlation between isophotal shapes and the luminosity of ellipticals. Khoshroshahi et al. (2006) have investigated the profile shapes of the central ellipticals in seven fossil systems with the conclusion that the isophote shapes of ellipticals in fossil groups are different compared to the brightest central galaxies in non-fossil systems, especially rich clusters. Luminous elliptical galaxies in non-fossil systems do not present discy isophotes (Kormendy & Bender 1996). In contrast, the brightest ellipticals in fossil groups show discy and boxy isophotes in similar proportions. If the central ellipticals in groups have indeed formed via the merging of all other major galaxies, then some of these merging events would have been gas rich, since groups are known to consist of a large spiral fraction. The discy characteristics of central ellipticals in fossil groups would then be consistent with numerical simulations, that discy isophotes result from gas-rich mergers. The difference in the observed isophote shapes of fossil group central galaxies and the brightest cluster galaxies does not rule out the possible evolutionary link of infalling pre-processed merged ellipticals from groups in clusters, however. This could still be the case if these ellipticals have undergone later gas-free mergers within the cluster environment. Moreover, about 40% of the brightest cluster galaxies exhibit at least one sec-

ondary nucleus, strongly supporting the idea of late mergers within the cluster environment. Further investigation of the isophote shape characteristics of central ellipticals in fossil groups will help to confirm or question the existing results and will shed more light on the evolution of fossil group central ellipticals and possible connection to the brightest cluster galaxies.

2.4 Scaling relations in fossil groups

The first study of the scaling properties of fossil groups compared to ordinary groups and clusters was carried out by Khoshroshahi et al. (2007). Based upon Chandra X-ray observations as well as optical imaging and spectroscopy this study comprised the information of seven fossil groups showing regular, symmetric X-ray emission, indicating no recent mergers. Scaling relations focusing on the total gravitational mass, X-ray temperature, X-ray luminosity, group velocity dispersion and the optical luminosity were studied. For a given optical luminosity of the whole group, fossil systems turn out to be more X-ray luminous than non-fossil groups. Focusing on the $L_X - T_X$ relation, fossils cannot be distinguished from ordinary groups or clusters, however. Fossils also show that for a given group velocity dispersion, X-ray luminosity and temperature are higher compared to non-fossil systems. The $M_X - T_X$ relation suggests that fossils are hotter, for a given total gravitational mass, consistent with an early formation epoch.

3 The search for new fossil group candidates

Complementary to the previous work on fossil groups as highlighted in section 2, the attempt to identify new fossil structures was made by the authors. This undertaking seems reasonable since the space densities of fossil groups determined so far suggest that these systems are as abundant as Hickson compact groups while the actual catalogue comprises only a negligible fraction compared to HCGs. The Λ CDM concordance model ($\Omega_m = 0.3$, $\Omega_\Lambda = 0.7$, $H_0 = 70 \text{ km s}^{-1}$) was used throughout this work. Luminosity distances D_L and angular diameter distances D_A have been calculated via the *Cosmology Calculator* (Wright 2006). In order to identify new fossil group candidates, the Sloan Digital Sky Survey and Rosat All Sky Survey have been cross-correlated to shortlist candidates of interest that meet the classification criteria as proposed by Jones et al. (2003). The query was defined via Structured Query Language (SQL). A similar approach has been carried out by Santos et al. (2007) focusing on different selection criteria, however. The query presented here focuses on intrinsically bright $M_{r'} \leq -21 + 5 \log h$, $\text{red } g' - r' > 0.8$ galaxies relating to ellipticals. The lower limit in absolute magnitude was ensured by calculating the corresponding apparent magnitudes via luminos-

ity distances D_L derived from the SDSS spectroscopic redshifts of the central ellipticals

$$m < M + 25 + 5 \log \left[\frac{D_L}{h^{-1} \text{Mpc}} \right] + A + K(z) \quad (2)$$

accounting for galactic extinction A and K -correction too. Only galaxies with an entry in the SDSS ROSAT table were considered for the further shortlisting of fossil group candidates. The associated X-ray component had to be extended with a ROSAT extent parameter of at least one arc-second. This value does not reflect the true extent of the X-ray source but gives the excess over the ROSAT point-spread function. Furthermore the distance of the ROSAT source had to be less than 100kpc from the central elliptical accounting also for the ROSAT position error. The SQL code is given in appendix A. The resulting sample was finally shortlisted via the 2^{mag} criterion forcing all systems to have no galaxies with $\Delta m_{1,2} \geq 2.0$ mag in the SDSS r' band within one-half virial radius. In contrast to the work of Santos et al. (2007) who use a constant value of $0.5h^{-1}$ Mpc for half the virial radius, the description of Evrard et al. (1996)

$$r_{\text{vir}} = 1.945 \cdot \left(\frac{T}{10 \text{keV}} \right)^{1/2} (1+z)^{-3/2} \cdot h^{-1} \text{Mpc} \quad (3)$$

as used by Jones et al. (2003) was applied here assuming a lower limit of the X-ray temperature of fossil groups of 0.7 keV. The 2^{mag} criterion was accounted for via an SDSS SQL function (see appendix A). The remaining objects were checked for morphology. Five galaxies were identified as spirals while three objects have been found in the vicinity of bright stars. These systems have been excluded from the sample leaving a final list of 34 previously nondetected fossil group candidates. The query also reidentified objects listed in the Santos et al. (2007) sample. However, many objects could not be reidentified since the procedure used here excludes all galaxies within half the virial radius not taking into account possible background galaxies, thus eliminating possible fossil group candidates that would pass the 2^{mag} criterion if group memberships were known. This indicates that there might be far more fossil candidates in our query when accounting also for group memberships via photometric redshifts. Table 3 gives coordinates as well as SDSS and ROSAT identifications of the new fossil group candidates. Table 4 presents the most important properties of the fossil group central ellipticals as well as the associated ROSAT X-ray component. Fig. 5 shows a colour-magnitude diagram of the newly found fossil group central ellipticals as well as the Santos et al. (2007) sample. The symbol size indicates the prominence of the associated X-ray source, visualizing the ROSAT extent/ Δ ratio as presented in Table 4. Arrows point to galaxies that have been observed with the William Herschel Telescope (WHT) and the Very Large Telescope (VLT). In order to get a glimpse on the optical luminosity function (OLF) of the newly detected fossil group candidates, SDSS photometric and spectroscopic redshifts,

when available, have been used to estimate group memberships and construct an OLF for all systems. Some of the OLFs confirm the lack of faint galaxies as previously observed by Mendes de Oliveira et al. (2006) while most of the systems don't show a dip in the OLF at fainter magnitudes. Fig. 4 presents the photometrically selected OLF of RX J1520.9+4840 from the new list of fossil aggregates. A clear dip in the OLF is visible around $M_{i'} = -18$. It has to be kept in mind, however, that this result is based upon photometric redshifts which exhibit far larger errors than spectroscopic measurements necessitating the use of multi-object spectroscopy of the faint galaxy population to confirm the lack of faint galaxies in fossil galaxy groups.

4 Observations

Table 2 summarizes the observations at the WHT and VLT that have been carried out to complement the existing data on fossil groups. Long-slit spectra have been obtained with the ISIS spectrograph at the WHT to measure Lick-IDS indices (Worthey et al. 1994) of the central ellipticals from both the new sample as well as fossil groups from the literature. These measurements will yield radial profiles of ages and metallicities of the central elliptical stellar populations that are supposed to contain the merger history of the whole group. It is then feasible to study how uniform the process of coalescence occurred in these systems and if fossil group central ellipticals are indeed the progenitors of brightest cluster galaxies (BCGs) or show similar stellar populations as found in non BCGs. In addition, VIMOS observations in service mode have been carried out at VLT UT3 Melipal to study the OLF of one fossil aggregate. Spectroscopic targets have been selected via SDSS magnitudes to determine the OLF down to $i' \sim 20$ corresponding to $M_{i'} \sim -17$. This magnitude limit ensures to identify a dip in the OLF around $M_{i'} \sim -18$ if present. Fig. 3 shows the VIMOS pre-image of the central elliptical of the fossil group candidate RX J1548.9+0851. The image reveals shells around the central elliptical that would confirm the idea of the system being the remainder of multiple merging events. The aquired data from the WHT and the VLT will shed more light on the formation process of fossil groups of galaxies complementing the few optical studies that have been carried out so far.

Acknowledgements. Paul Eigenthaler is supported by the University of Vienna in the frame of the Initiative Kolleg (IK) *The Cosmic Matter Circuit* I033-N.

References

- Adelman-McCarthy, J. et al.: 2008, ApJS 175 , 297
- Barnes, J.E.: 1989, Nature 338 , 123
- Beers, T. et al.: 1995, AJ 109 , 874
- Binney, J. & Tremaine, S.: 1987, Princeton University Press
- Chandrasekhar, S.: 1943, ApJ 97 , 255
- Cypriano, E.S. et al.: 2006, AJ 132 , 514

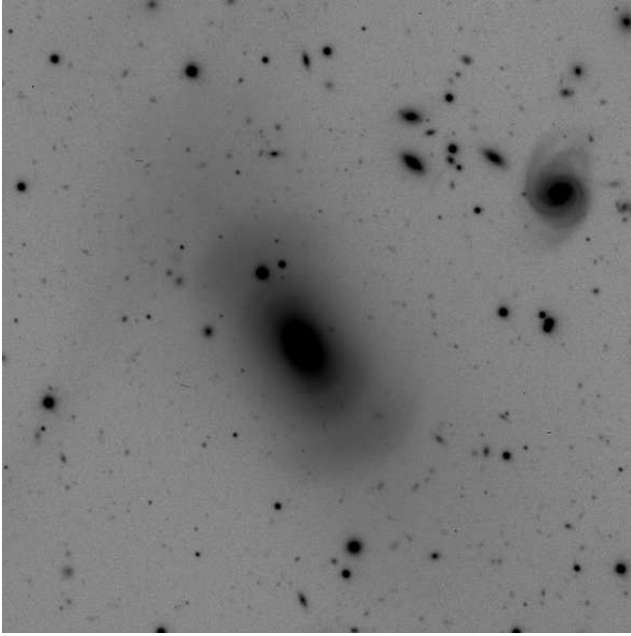


Fig. 3 VIMOS PRE-IMG of the fossil group candidate RX J1548.9+0851 from the Santos et al. (2007) sample. The bright spiral shows a redshift difference of $\Delta z \sim 0.008$ to the central elliptical and doesn't violate the 2^{mag} criterion. Shells can be clearly seen around the elliptical which suggest multiple past merging events that would confirm the status of RX J1548.9+0851 as a fossil group. North is up, east is to the left. The field of view is ~ 2 arcmin on a side.

Evrard, A.E. et al.: 1996, ApJ 469 , 494
 Gnedin, O.Y.: 2003, ApJ 589 , 752
 Geller, M.J., Huchra, J.P.: 1983, ApJS 52 , 61
 Hickson, P.: 1982, ApJ 255 , 382
 Hickson, P.: 1997, ARA&A 35 , 357
 Hunsberger, S.D. et al.: 1996, ApJ 462 , 50
 Jones, L.R. et al.: 2003, MNRAS 343 , 627
 Kalberla, P. et al.: 2005, A&A 440 , 775
 Khosroshahi, H.G. et al.: 2004, MNRAS 349 , 1240
 Khosroshahi, H.G. et al.: 2006, MNRAS 372 , 68
 Khosroshahi, H.G. et al.: 2007, MNRAS 377 , 595
 Kormendy, J., Bender, R.: 1996, ApJ 464 , 119
 Mendes de Oliveira, C. et al.: 2006, AJ 131 , 158
 Mendes de Oliveira, C. et al.: 2009, AJ 138 , 502
 Mukai, K.: 1993, Legacy 3 , 21
 Mulchaey, J.S.: 2000, ARA&A 38 , 289
 Naab, T., Burkert, A.: 2003, ApJ 597 , 893
 Naab, T., Khochfar, S., Burkert, A.: 2006, ApJ 636 , 81
 Nolthenius, R. & White, S.: 1987, MNRAS 225 , 505
 Ponman, T.J. et al.: 1994, Nature 369 , 462
 Santos, W.A. et al.: 2007, AJ 134 , 1551
 Sun, M. et al.: 2004, ApJ 612 , 805
 Tully, R.B.: 1987, ApJ 321 , 280
 Ulmer, M.P. et al.: 2005, ApJ 624 , 124
 Valotto, C.A. et al.: 2004, ApJ 603 , 67
 Vikhlinin, A. et al.: 1999, ApJ 520 , 1
 Voges, W. et al.: 1999, A&A 349 , 389
 Worthey, G. et al.: 1994, ApJS 94 , 687
 Wright, E.L.: 2006, PASP 118 , 1711
 Yoshioka, T. et al.: 2004, AdSpR 34 , 2525

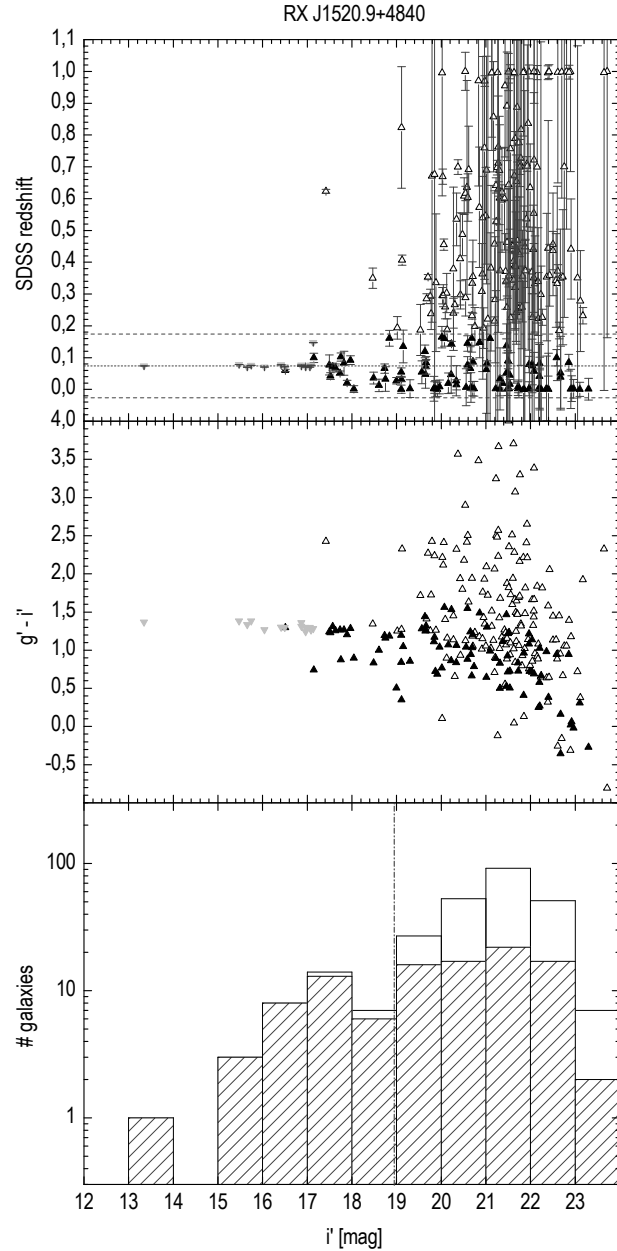


Fig. 4 Photometrically determined optical luminosity function of the fossil group candidate RX J1520.9+4840 from the new sample. All objects in the SDSS classified as galaxies within one-half virial radius are plotted. Upper panel: Open and black triangles represent SDSS photometric redshifts while gray triangles indicate SDSS spectroscopic redshifts. The dotted line indicates the spectroscopic redshift z of the central elliptical, while dashed lines at $z \pm \Delta z$ ($\Delta z = 0.1$; SDSS photometric redshift uncertainty) indicate borders for group membership. Mid panel: Colour-Magnitude Diagram of the investigated galaxy population. Galaxies exhibiting adequate photometric redshifts for group membership follow a red sequence as observed in ordinary groups. Lower panel: Photometrically-determined luminosity function. Blank histograms show all galaxies while dashed ones indicate objects within $z \pm \Delta z$. The dash dotted line corresponds to $M_{i'} = -18$. A dip in the photometrically selected OLF around $M_{i'} = -18$ is clearly visible.

Table 2 Fossil systems observed with the WHT and the VLT.

galaxy	α_{2000}	δ_{2000}	exposure [s]	resolution [\AA pix $^{-1}$]		date
<i>William Herschel Telescope^a</i>						
				blue	red	
RX J0752.7+4557	07 52 44.2	+45 56 57.4	3 × 3000	0.86	0.26	20.12.2008
RX J0844.9+4258	08 44 56.6	+42 58 35.7	3 × 3000	0.86	0.26	20.12.2008
NGC 1132	02 52 51.8	-01 16 28.8	4 × 2700	0.86	0.26	20.12.2008
RX J1548.9+0851	15 48 55.9	+08 50 44.4	3 × 2600	0.86	0.93	28.04.2009
RX J1520.9+4840	15 20 52.3	+48 39 38.6	3 × 2600	0.86	0.93	28.04.2009
RX J1152.6+0328	11 52 37.6	+03 28 21.8	3 × 2700	0.86	0.93	28.04.2009
<i>Very Large Telescope^b</i>						
RX J1548.9+0851	15 48 55.9	+08 50 44.4	4500	0.51		26.05.2009

^a Observations carried out in Visitor Mode.^b Observations carried out in Service Mode. The date refers to the completion of the last Observing Block (OB) for the given target.**Table 3** Fossil group candidates: ROSAT and SDSS identifications.

ID Number (1)	ROSAT Name (2)	SDSS α_{2000} ^a (3)	SDSS δ_{2000} ^a (4)	SDSS objid (5)
01.....	RXJ0159.8-0850	01 59 49.3	-08 49 58.8	587727884161581256
02.....	RXJ0725.7+3741	07 25 41.3	+37 40 27.7	587737826206482926
03.....	RXJ0730.3+3728	07 30 20.4	+37 27 40.8	587725775602450780
04.....	RXJ0801.0+3603	08 00 56.8	+36 03 23.6	587728905564258619
05.....	RXJ0825.9+0415	08 25 57.8	+04 14 48.3	587732702851170810
06.....	RXJ0826.9+3108	08 26 57.6	+31 08 04.9	587732469849325635
07.....	RXJ0909.9+3106	09 09 53.3	+31 06 03.2	588016878295318532
08.....	RXJ1005.8+1058	10 05 50.7	+10 58 11.7	587734949665243313
09.....	RXJ1006.1+0710	10 06 08.3	+07 10 29.5	587732579379904650
10.....	RXJ1030.5+1416	10 30 34.8	+14 15 41.8	587735349637349534
11.....	RXJ1041.8+5303	10 41 47.6	+53 03 41.4	587733081343656013
12.....	RXJ1055.1+4246	10 55 06.6	+42 45 24.4	588017626148634721
13.....	RXJ1056.1+0252	10 56 06.6	+02 52 13.5	587726033315299465
14.....	RXJ1107.4+1245	11 07 24.2	+12 44 20.0	588017567629509093
15.....	RXJ1115.9+0130	11 15 51.9	+01 29 55.1	587728307491897590
16.....	RXJ1128.6+3530	11 28 34.4	+35 30 14.0	587739305286238362
17.....	RXJ1152.6+0328	11 52 37.6	+03 28 21.8	587726033858330762
18.....	RXJ1211.1+3520	12 11 08.3	+35 19 58.8	587739304216232052
19.....	RXJ1327.1+0212	13 27 01.0	+02 12 19.5	587726015078465728
20.....	RXJ1349.9+4217	13 49 51.1	+42 16 47.8	588017604154687567
21.....	RXJ1352.0+6105	13 51 58.3	+61 04 19.0	588011219135889619
22.....	RXJ1353.4+4424	13 53 20.3	+44 24 19.8	588298662507184284
23.....	RXJ1402.8+3431	14 02 46.6	+34 31 08.0	587739131880603717
24.....	RXJ1431.3-0054	14 31 21.2	-00 53 44.3	588848898855469518
25.....	RXJ1450.2+4134	14 50 08.3	+41 33 59.8	588017116130246662
26.....	RXJ1453.6+0359	14 53 38.5	+03 59 33.4	587726101487747355
27.....	RXJ1501.3+5455	15 01 18.0	+54 55 18.3	588011101565354082
28.....	RXJ1520.9+4840	15 20 52.3	+48 39 38.6	587735666921898155
29.....	RXJ1539.8+4143	15 39 51.4	+41 43 25.4	587733397568356378
30.....	RXJ1540.4+3622	15 40 23.0	+36 21 56.6	587736751928770630
31.....	RXJ1624.7+3727	16 24 43.4	+37 26 42.4	587735666392105305
32.....	RXJ1653.1+3909	16 53 07.8	+39 08 53.1	588007005270966692
33.....	RXJ1717.1+2931	17 17 06.9	+29 31 21.1	587729408084935169
34.....	RXJ2139.5-0722	21 39 28.5	-07 21 46.6	587726878878728621

^a Right ascension is given in hours, minutes, and seconds and declination is given in degrees, arcminutes, and arcseconds.

Table 4 Fossil group candidates: Properties of the central elliptical and the associated X-ray component.

ID Number (1)	central elliptical galaxy					ROSAT X-ray properties			
	redshift ^a (2)	i' ^a [mag] (3)	$g' - i'$ ^a [mag] (4)	$M_{i'}$ ^a [mag] (5)	$\frac{1}{2}r_{\text{vir}}^b$ [arcmin] (6)	Δ^c [arcsec] (7)	extent ^c [arcsec] (8)	extent/ Δ^c (9)	L_X (0.5-2keV) ^d [ergs s ⁻¹] (9)
01	0.405	17.29	2.00	-24.37	0.680	12.8	44	3.44	8.42E+44
02	0.425	17.34	2.58	-24.56	0.647	42.8	56	1.31	1.84E+44
03	0.200	17.58	1.69	-22.04	1.411	21.8	40	1.83	6.29E+43
04	0.287	16.13	2.23	-24.30	0.970	35.5	47	1.33	3.85E+44
05	0.225	15.81	2.01	-24.31	1.249	21.4	21	0.98	1.51E+44
06	0.209	15.26	1.92	-24.43	1.346	52.1	76	1.46	1.25E+44
07	0.272	16.57	1.20	-23.65	1.026	9.2	22	2.39	6.65E+44
08	0.162	15.15	1.68	-24.10	1.755	7.4	85	11.45	4.58E+43
09	0.202	17.25	1.35	-22.39	1.394	48.9	22	0.45	1.89E+43
10	0.317	16.23	2.31	-24.49	0.875	26.1	61	2.34	2.07E+44
11	0.187	16.52	1.71	-22.59	1.517	28.2	13	0.46	1.97E+43
12	0.371	18.57	1.48	-23.05	0.744	7.2	17	2.36	1.00E+44
13	0.236	17.60	1.28	-22.27	1.189	6.1	19	3.12	1.03E+45
14	0.420	17.93	2.46	-23.12	0.655	15.8	9	0.57	1.19E+44
15	0.352	17.19	2.03	-24.26	0.786	22.5	57	2.54	7.30E+44
16	0.402	17.59	2.52	-23.59	0.685	15.6	12	0.77	3.02E+44
17	0.081	14.25	1.38	-23.06	3.600	27.4	71	2.59	1.08E+43
18	0.136	15.14	1.58	-23.52	2.097	35.8	52	1.45	4.11E+43
19	0.260	16.26	2.16	-24.11	1.075	40.5	58	1.43	2.30E+44
20	0.289	17.67	1.92	-22.77	0.964	8.2	19	2.30	1.08E+44
21	0.323	17.32	2.34	-23.47	0.858	23.2	6	0.26	3.61E+43
22	0.152	17.03	1.37	-21.48	1.873	24.1	9	0.37	1.23E+43
23	0.175	17.14	1.31	-22.61	1.619	6.7	10	1.49	1.28E+43
24	0.403	17.49	2.70	-23.80	0.684	43.1	52	1.21	2.27E+44
25	0.157	14.89	1.65	-24.02	1.818	35.9	54	1.50	2.24E+43
26	0.370	16.82	2.35	-24.24	0.746	36.1	42	1.16	2.33E+44
27	0.339	17.24	1.83	-23.63	0.818	7.3	15	2.05	1.54E+44
28	0.074	13.35	1.37	-24.12	3.933	31.4	71	2.26	4.35E+43
29	0.119	14.83	1.55	-23.96	2.404	10.3	12	1.17	7.06E+42
30	0.231	16.53	1.76	-23.35	1.213	27.7	11	0.40	2.63E+43
31	0.199	16.89	1.79	-23.99	1.417	12.1	13	1.08	2.97E+43
32	0.147	15.70	1.64	-23.14	1.945	33.0	19	0.58	1.40E+43
33	0.278	16.95	1.68	-22.12	1.003	4.2	30	7.08	6.92E+44
34	0.410	17.58	2.50	-23.88	0.672	26.3	20	0.76	1.53E+44

^a Redshifts and magnitudes are taken from the SDSS DR 6.

^b Half the virial radius given in arcminutes. The virial radius was estimated via $r_{\text{vir}} = 1.945 \cdot \left(\frac{T}{10\text{keV}}\right)^{1/2} (1+z)^{-3/2} \cdot h^{-1}\text{Mpc}$ as used in Jones et al. (2003). For the X-ray temperature a lower limit of 0.7 keV was assumed.

^c ROSAT Δ and extent parameters. Δ gives the distance of the X-ray source to the central elliptical. Extent gives the excess of the detected X-ray source over the ROSAT PSF. The ratio extent/ Δ indicates the prominence of the X-ray source with larger values indicating more extended sources close to the central elliptical.

^d ROSAT X-ray luminosities. ROSAT countrates have been converted to X-ray fluxes via the tool PIMMS (Mukai, 1993) assuming a Raymond-Smith model with 2keV and a metallicity of $Z = 0.4Z_{\odot}$. HI column densities of the Leiden/Argentine/Bonn (LAB) Survey of Galactic HI (Kalberla et al. 2005) were taken into account to determine extinction-free fluxes.

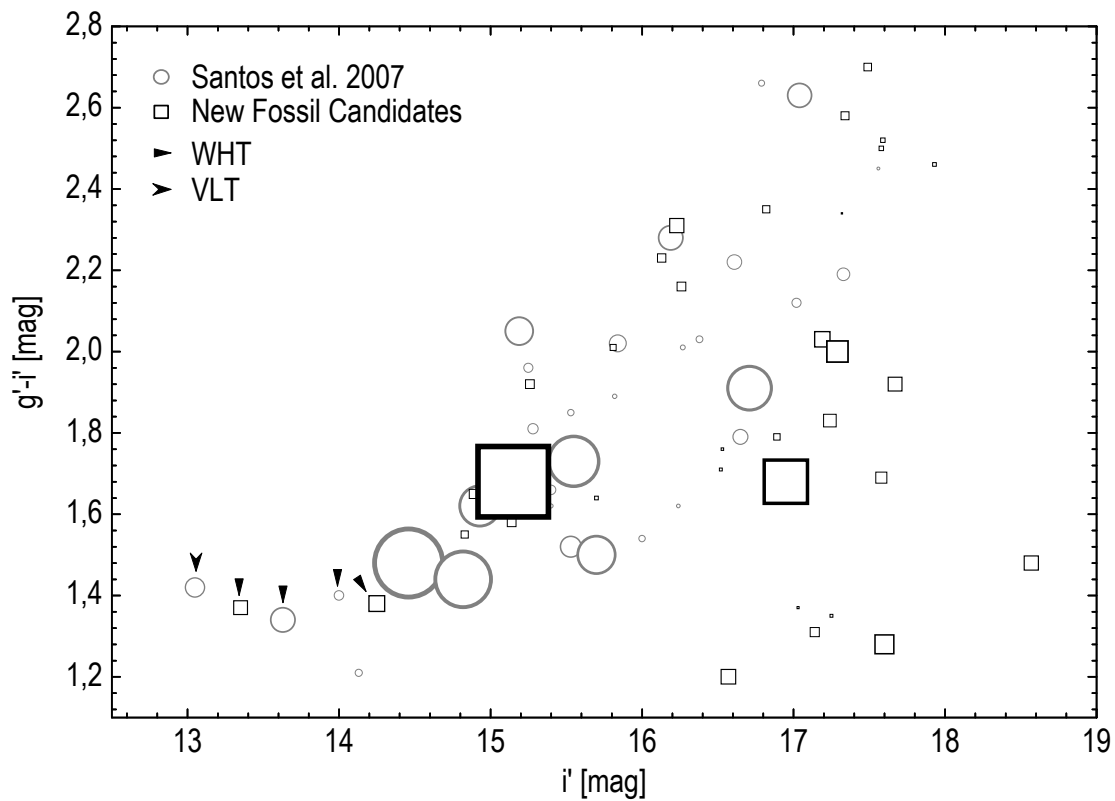


Fig. 5 Colour-magnitude diagram for the central elliptical galaxies of fossil structures identified in the SDSS. Circles show the list of Santos et al. (2007) while squares represent new structures identified by the authors. The arrows point to objects that have been observed with the WHT and the VLT by the authors. The size of the symbols indicates the extent/ Δ ratio as presented in Table 4.

A SQL Query

SQL query used within SDSS DR6 to select the fossil group candidates listed in Table 3.

```
SELECT p.objid, s.z, p.ra, p.dec, p.r, p.g-p.r, r.delta, r.cps, r.cpserr, r.extent
FROM specobj s, photoobj p, rosat r
WHERE s.bestobjid= p.objid
```

Selection of objects that have been spectroscopically classified as galaxies with $z \leq 0.5$ and show an entry in the SDSS ROSAT table.

```
AND s.specclass = 2
AND p.objid= r.objid
AND s.z BETWEEN 0.0 AND 0.50
```

Selection of bright ($M_r \leq -21 + 5 \log h$), red ($g' - r' > 0.8$) galaxies via the relation: $m < M + 25 + 5 \log (D_L[\text{Mpc}] \cdot h) + A + K(z)$ ¹

```
AND p.r <
-21.0
+ 25 + 5*LOG10 ((-0.15958 + 4290.00033 *s.z + 3255.86186 *s.z*s.z - 1009.42877 *s.z*s.z*s.z) *0.7)
- 0.00554 + 1.31479 *s.z - 1.08771 *s.z*s.z + 5.09347 *s.z*s.z*s.z
+ p.extinction_r
AND p.g - p.r > 0.8
```

*Selecting galaxies with an extended X-ray source within 100kpc taking into account the ROSAT position error.*²

```
AND r.extent >= 1
AND r.delta <= 100/(0.00717 + 20.42378 *s.z - 21.97056 *s.z*s.z + 11.06756 *s.z*s.z*s.z) + r.poserr
```

*Identifying non-fossil systems. All objects within half the virial radius that are photometrically classified as galaxies and less than 2 mag fainter than the central elliptical are counted.*³

```
SELECT count(*)-1
FROM photoObj p, dbo.fGetNearbyObjEq(ra, dec, radius) n
WHERE p.objID = n.objID
AND p.type = 3
AND p.r - m1 < 2.0
```

¹ D_L and $K(z)$ were implemented via third order polynomials that were fit to the D_L and $K(z)$ data derived from the *Cosmology Calculator* and SDSS for redshifts up to $z = 0.5$. The `kcorr_r` entry in the SDSS photoz table was not directly used in the query since these values are based upon photometric redshifts which can strongly deviate from spectroscopic redshifts and would lead to wrong results. Therefore $K(z)$ was determined based upon galaxies with $g' - r' > 0.8$ that show hardly any difference in photometric and spectroscopic redshifts.

² The polynomial gives the angular scale as a function of redshift based upon angular diameter distances D_A .

³ This query has been performed for all galaxies shortlisted via the previous criteria. `ra`, `dec` give the coordinates of the central galaxy in decimal degrees while `radius` presents half the virial radius in arcminutes. `m1` stands for the r' band magnitude of the central galaxy.